PERGAMON

International Journal of Solids and Structures 40 (2003) 4895–4910

INTERNATIONAL JOURNAL OF SOLIDS and STRUCTURES

www.elsevier.com/locate/ijsolstr

Vertical correlations in superlattices using the Grinfeld method

A. Danescu [a,*], G. Grenet [b]

[a] *Departement Mécanique des Solides, CNRS-UMR 5513, Ecole Centrale de Lyon, 36 Avenue Guy de Collongue, BP 163 F-69131 Ecully Cedex, France*

[b] *LEOM, CNRS-UMR 5512, Ecole Centrale de Lyon, BP 163 F-69131 Ecully Cedex, France*

Received 18 May 2002; received in revised form 20 March 2003

Abstract

In this paper, we analyse the energetics of a multilayered structures like, for instance, $B/A/B/A_{substrate}$. It is well-known that a coherent pre-strained B layer on an A substrate will generally results in a corrugation of the free-surface of the B layer. This behavior is the result of stress relaxation in the B-layer and the phenomenon is known as the Asaro-Tiller-Grinfeld instability. We extend the methods used for a two-layer structure to a multilayered structure and the main application is the vertical correlation in superlattices. We analyse the energetics of a corrugated B layer which is grown on a $A/B/A_{substrate}$, where the A layers are flat but the intermediate B layer is already corrugated. We show that the self-organization of the second B layer, due to elastic interactions in the bulk, depends on the corrugation of the first B layer and the generic best situation is that of a top-on-top (also called correlated layers) vertical alignment. We also prove that the interaction energy between two successive B layers attains a maximum at a critical thickness of the intermediate A layer. This interaction energy has the same order of magnitude as the elastic energy release due to free-surface corrugation at each upper surface of a B layer.

Keywords: Super lattices; Instabilities; Strain

1. Introduction

Grinfeld's method (Grinfeld, 1986, 1991, 1993) turns out to be extremely fruitful to explain various kinds of instabilities in numerous fields of physics and chemistry. For example, if a coherent thin film is grown on a single-crystal substrate by advanced growth techniques such as molecular beam epitaxy (MBE) and if the film lattice parameter differs from that of the substrate by more than 2%, the thin film growth mode generally changes from a layer-by-layer two-dimensional (2D) mechanism to a three-dimensional (3D) mechanism leading to the formation of periodically auto-assembled islands. This phenomenon takes place when the film thickness has reached a critical value, i.e., the so-called 2D-to-3D growth mode threshold. In other words, such a coherent island formation is favourable only if it guarantees more misfit strain energy relief than the concomitant surface energy increase.

* Corresponding author. Tel.: +33-4-72186000; fax: +33-4-7618653.
E-mail address: danescu@ec-lyon.fr (A. Danescu).

0020-7683/03/$ - see front matter © 2003 Elsevier Ltd. All rights reserved.
doi:10.1016/S0020-7683(03)00172-0

In this paper, we will extend Grinfeld's approach to the case of a multi-layer heterostructure, viz., a periodic stack of thin films alternately made of two different mismatched materials on a semi-infinite substrate. Such a strained-layer superlattice is widely used in optoelectronical devices made from III–V semiconductors. It is presently well accepted that, when the multi-layer is a succession of coherently strained island layers (issued from 3D growth mode) and of spacer layers lattice-matched to the substrate, the strain distribution due to a buried island layer favours a top-on-top island growth (Xie et al., 1995; Tersoff et al., 1996; Springholz et al., 1998; Zhang et al., 1999; Priester, 2001) leading to a vertical alignment. For actual systems grown along (1 0 0) substrates, experiments in Solomon et al. (1996), Teichert et al. (1996), Legrand et al. (1999), Wu et al. (1997) and Lita et al. (1999) actually show this vertical alignment between islands belonging to successive layers. However, it has been recently claimed that this widely found vertical correlation could be affected by strong elastic anisotropy leading to non-top-on-top vertical island stacking (Spencer et al., 2001; Shchukin et al., 1998; Holý et al., 1999). Moreover, another study has shown that such a strained-layer superlattice can be either stable or unstable versus growth, and when unstable, the layer modulation can be in phase, out of phase or complexly related (Shilkrot et al., 2000).

Motivated by the above-mentioned underlying physics, our approach in this paper is based on a generalisation of Grinfeld's method (Grinfeld, 1991). It consists in a comparison between the elastic energy stored in a given multi-layered structure and that of a reference state, extending a previous result in Danescu (2001).

The paper is organized in two parts. The first is devoted to the continuum mechanics background and general results valid for multi-layered structures. The main energy estimate for two-layer materials is Eq. (1) which is straightforwardly extended to the case of multi-layered materials in Section 3.2. From a quantitative estimate we have studied, using a Fourier technique, a first order problem whose solution provides a valid result (Eq. (11)) for small amplitude perturbations. The second part is dedicated to applications in the semiconductor crystal growth field. The first case to be studied is the growth of a cap-layer on a strained film: we predict that, as a consequence of our energy estimate, the cap-layer regains 2D growth giving a flat cap-layer surface morphology. The second application deals with the controversial problem of correlation versus anti-correlation island organization in multi-layered heterostructures. We show that, in agreement with most experiments, correlation is the generic situation. As an additional result we show that there is an optimum spacer thickness in a periodic multi-layered heterostructure for maximum interaction between two successive strained layers.

2. Preliminaries

In this paper, we consider the case of a multi-layered material as illustrated in Fig. 1. The successive layers labelled $1,\ldots,L$ and heights $h_1,\ldots,h_L$ are alternately materials of types A and B on a semi-infinite substrate assumed by convention, to be of type A. Materials A and B belong to the same crystallographic space group but differ by lattice parameter. Moreover, all interfaces, labelled $\Sigma_1,\ldots,\Sigma_{L-1}$ (except the last-layer free-surface) are taken to be *coherent*. This means that the crystal lattices on contact are distorted in such a way to match each other on the interface even if they are lattice mismatched when in their natural (undistorted) configuration. Since our main application to physics concerns the III–V or IV semiconductors, both A and B are assumed to be linear elastic materials with cubic symmetry (zinc–blende for III–V semiconductors and diamond for IV semiconductors). Although the general results of Section 3 also hold for orthotropic materials (see Danescu, 2001), for simplicity, computations in the following are performed only for cubic materials.

To describe a *multi-layered structure with flat interfaces*, let us introduce the following notation: let $L \geqslant 1$ be an integer labelling successive layers; as explained above the successive interfaces, denoted Σ_i, are of type B/A for even i and of type A/B for odd i. Their vertical locations are denoted h_i with respect to the interface

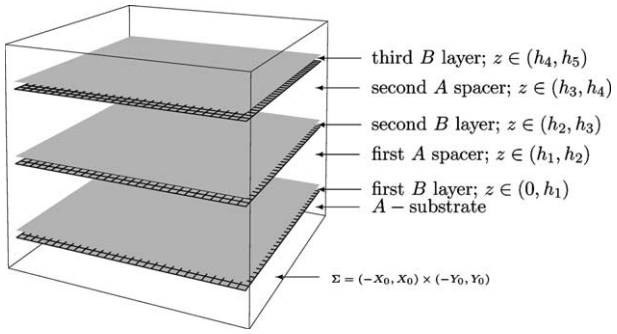

Fig. 1. Diagram of a multi-layered structure with flat interfaces: the meshed interfaces are B/A interfaces (denoted Σ_i for even i), while unmeshed ones, are B/A interfaces (denoted Σ_i for odd i). The thickness of a B layer is small compared to that of spacer layers A. The vertical positions of the interfaces, from the first interface $\mathrm{B/A_{substrate}}$ are respectively $h_1, h_2, \ldots$ and the lateral boundary is denoted S_0.

of the first B layer with the A substrate. Let Σ be a rectangle $(-X_0, X_0) \times (-Y_0, Y_0)$ and denote $\Omega_0 = \Sigma \times (0, h_L)$, $S_0 = \partial\Sigma \times (0, h_L)$, $\Omega_\alpha = \Sigma \times (h_{\alpha-1}, h_\alpha)$ and $\Sigma_\alpha = \Sigma \times h_\alpha$ for $\alpha = 1, \ldots, L$.

For the description of a *multi-layered structure with almost flat interfaces* we introduce L smooth functions $\Phi_\alpha : \Sigma \to \mathbb{R}$ with zero-mean value and Σ-periodic, and for convenience, we shall impose $\max_\Sigma |\Phi_\alpha| < \min(h_\alpha/2, h_{\alpha-1}/2)$ for $\alpha = 1, \ldots, L-1$ and $\max_\Sigma |\Phi_L| < h_L/2$. We denote $\hat{\Omega}_0 = \Sigma \times (0, h_L + \Phi_L)$, $\hat{S}_0 = \partial\Sigma \times (0, h_L + \Phi_L)$, $\hat{\Omega}_\alpha = \Sigma \times (h_{\alpha-1} + \Phi_{\alpha-1}, h_\alpha + \Phi_\alpha)$ and $\hat{\Sigma}_\alpha = \Sigma \times (h_\alpha + \phi_\alpha)$ for $\alpha = 1, \ldots, L$. The condition regarding the mean value imposed on functions Φ_α expresses the fact that the amount of material in both situations, with flat interfaces and with almost flat interfaces, is the same.

For a linear elastic material with cubic symmetry group and preferred axes (x, y, z) the Hooke tensor has the general form

$$H_{ijkl} = \lambda\delta_{ij}\delta_{kl} + \mu(\delta_{ik}\delta_{jl} + \delta_{il}\delta_{jk}) + \eta(\delta_{ix}\delta_{jx}\delta_{kx}\delta_{lx} + \delta_{iy}\delta_{jy}\delta_{ky}\delta_{ly} + \delta_{iz}\delta_{jz}\delta_{kz}\delta_{lz}),$$

thus, the non-zero components of the Hooke tensor are (up to well-known permutations due to the symmetry) in cartesian coordinates

$$H_{xxxx} = H_{yyyy} = H_{zzzz} = \lambda + 2\mu + \eta,$$

$$H_{xxyy} = H_{xxzz} = H_{yyzz} = \lambda,$$

$$H_{xyxy} = H_{xzxz} = H_{yzyz} = 2\mu.$$

In the following we shall use $(\mathbf{H}^{\mathrm{A}}, \lambda_{\mathrm{A}}, \mu_{\mathrm{A}}, \eta_{\mathrm{A}})$ and $(\mathbf{H}^{\mathrm{B}}, \lambda_{\mathrm{B}}, \mu_{\mathrm{B}}, \eta_{\mathrm{B}})$, to denote the elastic constants in materials A and B respectively.

To take into account the misfit between materials A and B, the constitutive relations between the Cauchy stress tensor, denoted $\boldsymbol{\sigma}$, and the strain tensor, denoted $\boldsymbol{\epsilon}$, are supposed to hold in the form

$$\boldsymbol{\sigma} = \mathbf{H}^{\mathrm{A}}[\boldsymbol{\epsilon}]$$

in the substrate and even-numbered layers (i.e., in material A), and

$$\boldsymbol{\sigma} = \mathbf{H}^{\mathrm{B}}[\boldsymbol{\epsilon} + \boldsymbol{\epsilon}^0]$$

in odd-numbered layers (i.e., in material B). The *misfit strain* $\boldsymbol{\epsilon}^0$ takes into account the mismatch between materials A and B only on its in-plane (x, y) components. Thus, in a configuration where *all interfaces are flat*, the vertical deformation will be such that the vertical *misfit stress* $\boldsymbol{\sigma}^{\mathrm{B}}\mathbf{e}_z = \mathbf{H}^{\mathrm{B}}[\boldsymbol{\epsilon}^0]\mathbf{e}_z$ vanishes. If we denote $\epsilon^0_{xx} = \epsilon^0_{yy} = m$, considering as usual that the misfit shear vanishes, i.e., $\epsilon^0_{xy} = 0$, a straightforward computation shows that the misfit stress is such that $\sigma_{zz} = \sigma_{xy} = \sigma_{xz} = \sigma_{yz} = 0$, and

$$\sigma^0_{xx} = \sigma^0_{yy} = \sigma^0 = m\left[2\lambda + 2\mu + \eta - \frac{2\lambda^2}{\lambda + 2\mu + \eta}\right].$$

Consequently, with flat interfaces, we are in a typical *plane stress* situation where

$$\boldsymbol{\epsilon} = m\begin{bmatrix} 1 & 0 & 0 \\ 0 & 1 & 0 \\ 0 & 0 & \dfrac{-2\lambda}{\lambda + 2\mu + \eta} \end{bmatrix}, \qquad \boldsymbol{\sigma} = \sigma^0\begin{bmatrix} 1 & 0 & 0 \\ 0 & 1 & 0 \\ 0 & 0 & 0 \end{bmatrix},$$

also called the *pseudomorphic* case by physicists.

3. Energy estimates for heterostructures

3.1. Estimate for the bulk energy

We start with the simplest case of a two-layer material, i.e. a structure A/B on an A substrate, also denoted in the following by $A/B/A_{substrate}$. Following an idea fully developed in Danescu (2001), we shall compare the elastic energy stored in a structure with flat interfaces, denoted in the following W_0, with the elastic energy stored in the same structure but with almost flat interfaces, denoted W_2.

In the reference case, the elastic energy W_0 can be computed once we have the solution to the following boundary value problem

($\mathscr{P}_0$): Find $\mathbf{u} : \Omega_0 \to \mathbb{R}^3$ solution of

(a) $\operatorname{div}\boldsymbol{\sigma} = 0$ in Ω_0,
(b) $\boldsymbol{\sigma}\mathbf{n} = 0$ on Σ_2,
(c) $\mathbf{u} = 0$ on Σ_0,
(d) $\mathbf{u} = \mathbf{u}^{\text{per.}}$ and $\mathbf{t} = \mathbf{t}^{\text{aper.}}$ on S_0,
(e) $[\![\mathbf{u}]\!] = 0$ on Σ_1,
(f) $[\![\boldsymbol{\sigma}]\!]\mathbf{n} = 0$ on Σ_1,

where $\mathbf{u}^{\text{per.}}$ and $\mathbf{t}^{\text{aper.}}$ are respectively a Σ-periodic and a Σ-anti-periodic boundary conditions.

Under previous assumptions, the unique solution of problem ($\mathscr{P}_0$) is $\mathbf{u} = 0$, i.e. *the relaxation is vertical* and the stored elastic energy is easily shown to be

$$W_0 = \frac{\operatorname{vol}(\Omega_1)}{2}\mathbf{H}^{\mathrm{B}}[\boldsymbol{\epsilon}^0] : \boldsymbol{\epsilon}^0.$$

In the case of almost flat interfaces, in order to compute the stored elastic energy W_2, one has to solve the boundary value problem

($\mathscr{P}_2$): Find $\mathbf{u} : \hat{\Omega}_0 \to \mathbb{R}^3$ solution of

(a) $\operatorname{div}\boldsymbol{\sigma} = 0$ in $\hat{\Omega}_0$,
(b) $\boldsymbol{\sigma}\mathbf{n} = 0$ on $\hat{\Sigma}_2$,
(c) $\mathbf{u} = 0$ on Σ_0,
(d) $\mathbf{u} = \mathbf{u}^{\text{per.}}$ and $\mathbf{t} = \mathbf{t}^{\text{aper.}}$ on S_0,
(e) $[\![\mathbf{u}]\!] = 0$ on $\hat{\Sigma}_1$,
(f) $[\![\boldsymbol{\sigma}]\!]\mathbf{n} = 0$ on $\hat{\Sigma}_1$,

but obviously, the unique solution of this problem is not $\mathbf{u} = 0$. Grinfeld's method allows W_2 to be computed by comparison with W_0 as follows: note that, by definition

$$W_2 = \frac{1}{2}\int_{\hat{\Omega}_1} \mathbf{H}^{\mathrm{B}}[\boldsymbol{\epsilon}+\boldsymbol{\epsilon}^0] : (\boldsymbol{\epsilon}+\boldsymbol{\epsilon}^0)\,\mathrm{d}V + \frac{1}{2}\int_{\hat{\Omega}_2} \mathbf{H}^{\mathrm{A}}[\boldsymbol{\epsilon}] : \boldsymbol{\epsilon}\,\mathrm{d}V.$$

So that integrating by parts, using the equilibrium equations and the periodicity conditions on the lateral surfaces, we have

$$W_2 = \frac{1}{2}\int_{\partial\hat{\Omega}_1} \boldsymbol{\sigma}^{\mathrm{B}}\mathbf{n}\cdot(\mathbf{u}+\boldsymbol{\epsilon}^0\mathbf{x})\,\mathrm{d}A + \frac{1}{2}\int_{\hat{\Sigma}_1} \boldsymbol{\sigma}^{\mathrm{A}}\mathbf{n}\cdot\mathbf{u}\,\mathrm{d}A.$$

Using the jump conditions on interface $\hat{\Sigma}_1$, the periodicity and the boundary conditions, we obtain

$$W_2 = \frac{1}{2}\int_{\partial\hat{\Omega}_1} \boldsymbol{\sigma}^{\mathrm{B}}\mathbf{n}\cdot\boldsymbol{\epsilon}^0\mathbf{x}\,\mathrm{d}A,$$

and again integrating by parts

$$W_2 = \frac{1}{2}\int_{\hat{\Omega}_1} \boldsymbol{\sigma}^{\mathrm{B}} : \boldsymbol{\epsilon}^0\,\mathrm{d}V.$$

In addition, the symmetry of the Hooke tensor gives

$$W_2 = \frac{1}{2}\int_{\hat{\Omega}_1} \mathbf{H}^{\mathrm{B}}[\boldsymbol{\epsilon}^0] : \boldsymbol{\epsilon}^0\,\mathrm{d}V + \frac{1}{2}\int_{\partial\hat{\Omega}_1} \mathbf{u}\cdot\mathbf{H}^{\mathrm{B}}[\boldsymbol{\epsilon}^0]\mathbf{n}\,\mathrm{d}A,$$

so that, we easily obtain: [1]

$$W_2 = W_0 + \frac{1}{2}\boldsymbol{\sigma}^0 : \int_{\hat{\Sigma}_1} \mathbf{u}\otimes\mathbf{n}\,\mathrm{d}A. \tag{1}$$

This result shows that only the values of the displacement at the interface $\hat{\Sigma}_1$ contribute to the difference $W_0 - W_2$. This means that whatever the displacements at the upper-surface $\hat{\Sigma}_2$ (that surface is stress-free), the difference $W_0 - W_2$ will not be affected. The physical interpretation of this result will be fully discussed in the second part of this paper but let us just note here that there will be no reason for corrugations to appear at the free-surface $\hat{\Sigma}_2$ (upper surface of the first A layer) because the surface energy will always tend to smooth the free-surface.

3.2. Energy estimates for multi-layer materials

The computation leading to formula (1) can be easily generalized to an arbitrary number of layers. Using the method detailed above a straightforward computation provides the following general estimate for the elastic stored energy:

1. For even L:

$$\hat{W} = W_0 + (-1)^{i+1}\frac{1}{2}\boldsymbol{\sigma}^0 : \sum_{i=1}^{L-1}\int_{\hat{\Sigma}_i} \mathbf{u}\otimes\mathbf{n}. \tag{2}$$

2. For odd L:

$$\hat{W} = W_0 + (-1)^{i+1}\frac{1}{2}\boldsymbol{\sigma}^0 : \sum_{i=1}^{L}\int_{\hat{\Sigma}_i} \mathbf{u}\otimes\mathbf{n}. \tag{3}$$

By convention, in (2) and (3) all normal fields $\mathbf{n}_i$ are oriented toward $\hat{\Omega}_{i+1}$.

[1] We use $\boldsymbol{a}\otimes\boldsymbol{b}$ for the second-order tensor that acts on a vector $\boldsymbol{v}$ as $(\boldsymbol{a}\otimes\boldsymbol{b})\boldsymbol{v} = (\boldsymbol{b}\cdot\boldsymbol{v})\boldsymbol{a}$.

3.3. Small amplitude 3D perturbations

In order to use (1) for a quantitative estimate of the second term in the right-hand side one has to solve the full problem $\mathscr{P}_2$. Although this is a straightforward task (e.g., using numerical tools) for a two-layer heterostructure because of the linearity of the problem, for multi-layered structures, it appears to be a problem of fast increasing complexity in the full three-dimensional formulation. However, for almost flat interfaces the second term in (1) is small, favouring an approximate estimate using a linearized version of the problem $\mathscr{P}_2$.

Therefore, we shall consider solution $\mathbf{u}$ of $\mathscr{P}_2$ as a small perturbation of solution $\mathbf{u} = 0$ of $\mathscr{P}_0$, i.e.

$$\mathbf{u} = \varepsilon\overline{\mathbf{u}}$$

and linearize problem $\mathscr{P}_2$ as follows: we fix *small* Σ-periodic functions $\varepsilon\Phi_1(x,y)$ and $\varepsilon\Phi_2(x,y)$, so that the normals $\mathbf{n}_1$ and $\mathbf{n}_2$ to $\hat{\Sigma}_1$ and $\hat{\Sigma}_2$, respectively, are

$$\hat{\mathbf{n}}_\alpha = \mathbf{e}_z + \varepsilon\overline{\mathbf{n}}_\alpha, \tag{4}$$

for $\alpha = 1$ or 2. The linearized version for the problem $\mathscr{P}_2$ is

($\overline{\mathscr{P}}_2$): Find $\overline{\mathbf{u}} : \Omega_0 \to \mathbb{R}^3$ solution of the boundary value problem:

(a) $\mathrm{div}\overline{\boldsymbol{\sigma}} = 0$ in Ω_0,
(b) Condition $(\mathscr{P}_2) - (b)$ becomes $\overline{\boldsymbol{\sigma}}\hat{\mathbf{n}}_2 = 0$ on $\hat{\Sigma}_2$, and gives at the first order

$$H^{\mathrm{A}}[\overline{\boldsymbol{\epsilon}}^{\mathrm{A}}]\mathbf{e}_z = 0 \quad \text{on } \Sigma_2,$$

(c) $\overline{\mathbf{u}} = 0$ on Σ_0,
(d) $\overline{\mathbf{u}} = \mathbf{u}^{\mathrm{per.}}$ and $\overline{\mathbf{t}} = \mathbf{t}^{\mathrm{aper.}}$ on S_0,
(e) $[\![\overline{\mathbf{u}}]\!] = 0$ on Σ_1,
(f) Condition $(\mathscr{P}_2) - (f)$ is equivalent to

$$\left[\varepsilon\mathbf{H}^{\mathrm{A}}[\overline{\boldsymbol{\epsilon}}^{\mathrm{A}}] - \varepsilon\mathbf{H}^{\mathrm{B}}[\overline{\boldsymbol{\epsilon}}^{\mathrm{B}} + \boldsymbol{\epsilon}^0]\right]\hat{\mathbf{n}}_1 = 0$$

and taking into account (4) and the fact that $\boldsymbol{\sigma}^0\mathbf{e}_z = \mathbf{H}^{\mathrm{B}}[\boldsymbol{\epsilon}^0]\mathbf{e}_z = 0$, one finds that, at the first order, on Σ_1 we have

$$\left(\mathbf{H}^{\mathrm{A}}[\overline{\boldsymbol{\epsilon}}^{\mathrm{A}}] - \mathbf{H}^{\mathrm{B}}[\overline{\boldsymbol{\epsilon}}^{\mathrm{B}}]\right)\mathbf{e}_z = \boldsymbol{\sigma}^0\overline{\mathbf{n}}_1.$$

Finally, note that the small-amplitude approximation is pertinent for semiconductor nanostructures obtained by 2D–3D growth mode transition because usually:

(i) the periodicity in the (x,y)-plane of the B-layers is $\sim$300 Å (attributed to strained-induced lateral auto-organization of so-grown nanostructures),
(ii) while the undulated part of the B-layer is $\sim$10–20 Å high,
(iii) the thickness of the spacer (A-layers) is in the $\sim$50–300 Å range.

3.4. Fourier analysis for the linearized problem

For the linearized problem $\overline{\mathscr{P}}_2$ that has been just established we shall use a Fourier series technique, and the energy estimate (1) becomes

$$\overline{W}_2 = W_0 + \frac{\varepsilon^2}{2}\boldsymbol{\sigma}^0 : \int_{\Sigma_1} \overline{\mathbf{u}} \otimes \overline{\mathbf{n}}\,\mathrm{d}A. \tag{5}$$

First, consider the development in double Fourier series in the generic case of a (x,y)-periodic function Φ (either Φ_1, Φ_2, or any Φ_α in the multi-layered case) on $[0,2\pi]\times[0,2\pi]$ as

$$\Phi(x,y)=\sum_{n,m=0}^{\infty}\lambda_{nm}[A_{nm}\cos(nx)\cos(my)+B_{nm}\sin(nx)\cos(my)+C_{nm}\cos(nx)\sin(my)+D_{nm}\sin(nx)\sin(my)],$$

where the coefficients λ_{nm} are defined by

$$\lambda_{nm}=\begin{cases}1/4 & \text{for } n=m=0,\\ 1/2 & \text{for } n=0,\ m\geqslant 1 \quad \text{or } m=0,\ n\geqslant 1,\\ 1 & \text{for } n\geqslant 1,\ m\geqslant 1\end{cases}$$

and the (n,m) components of the Fourier series of Φ are defined as usual as

$$A_{nm}=\frac{1}{\pi^2}\int_{[0,2\pi]\times[0,2\pi]}\Phi(x,y)\cos(nx)\cos(my)\,\mathrm{d}x\,\mathrm{d}y,$$

$$B_{nm}=\frac{1}{\pi^2}\int_{[0,2\pi]\times[0,2\pi]}\Phi(x,y)\sin(nx)\cos(my)\,\mathrm{d}x\,\mathrm{d}y,$$

$$C_{nm}=\frac{1}{\pi^2}\int_{[0,2\pi]\times[0,2\pi]}\Phi(x,y)\cos(nx)\sin(my)\,\mathrm{d}x\,\mathrm{d}y,$$

$$D_{nm}=\frac{1}{\pi^2}\int_{[0,2\pi]\times[0,2\pi]}\Phi(x,y)\sin(nx)\sin(my)\,\mathrm{d}x\,\mathrm{d}y.$$

In the following, we shall use the compact notation

$$\Phi=\sum_{n,m=0}^{\infty}\Phi_{nm}\cdot T_{nm},$$

where Φ_{nm} denotes the (n,m) component of Φ given by

$$\Phi_{nm}=\lambda_{nm}(A_{nm},B_{nm},C_{nm},D_{nm})$$

and T_{nm} is defined as

$$T_{nm}=(\cos(nx)\cos(my),\sin(nx)\cos(my),\cos(nx)\sin(my),\sin(nx)\sin(my)).$$

The first-order derivatives ∂_x and ∂_y act as linear applications on a generic scalar function Φ and if we introduce

$$D_x=\begin{bmatrix}0&1&0&0\\-1&0&0&0\\0&0&0&1\\0&0&-1&0\end{bmatrix},\qquad D_y=\begin{bmatrix}0&0&1&0\\0&0&0&1\\-1&0&0&0\\0&-1&0&0\end{bmatrix},$$

we have $(D^x)^2=-\mathbf{I}$, $(D^y)^2=-\mathbf{I}$, and $\partial_x\Phi=\sum_{n,m=0}^{\infty}n(D_x\Phi_{nm})\cdot T_{nm}$, $\partial_y\Phi=\sum_{n,m=0}^{\infty}m(D_y\Phi_{nm})\cdot T_{nm}$.

Finally, note that although the functions Φ_α are defined on $[0,2\pi]^2$, we actually have an (x,y)-periodicity on a typical domain $[-X_0,X_0]\times[-Y_0,Y_0]$. In that case the Fourier coefficients have to be computed as

$$\hat{A}_{nm}=\frac{1}{X_0Y_0}\int_{\Sigma}\Phi(x,y)\cos\left(n\pi\frac{x}{X_0}\right)\cos\left(n\pi\frac{y}{Y_0}\right)\mathrm{d}x\,\mathrm{d}y$$

and similar expressions for $\widehat{B}_{nm}$, etc. The only change to be made in the formalism presented above concerns the form of the coefficients of the differential operators ∂_x and ∂_y, where n and m should be replaced by $n\pi/X_0$ and $m\pi/Y_0$, respectively.

Turning back to our main purpose, the general field equations are

$$(\lambda+2\mu+\eta)u_{x,xx}+\mu(u_{x,yy}+u_{x,zz})+(\lambda+\mu)(u_{y,yx}+u_{z,zx})=0, \tag{6}$$

$$(\lambda+2\mu+\eta)u_{y,yy}+\mu(u_{y,xx}+u_{y,zz})+(\lambda+\mu)(u_{x,xy}+u_{z,zy})=0, \tag{7}$$

$$(\lambda+2\mu+\eta)u_{z,zz}+\mu(u_{z,xx}+u_{z,xx})+(\lambda+\mu)(u_{y,yz}+u_{x,xz})=0. \tag{8}$$

Each projection on the (n,m)-component of a double Fourier series becomes a coupled system of ordinary differential equations completed by the boundary conditions and interface conditions.

We denote by $\overline{\mathbf{u}}_{nm}$ the (n,m) component of displacement $\overline{\mathbf{u}}$, i.e.,

$$\overline{\mathbf{u}}_{nm}=(U^x_{nm}(z)\cdot T_{nm},U^y_{nm}(z)\cdot T_{nm},U^z_{nm}(z)\cdot T_{nm}),$$

which introduces 12 unknown functions. It is straightforward to rewrite the field equations as

$$\mathbf{M}_{nm}\mathbf{U}''_{nm}+\mathbf{N}_{nm}\mathbf{U}'_{nm}+\mathbf{P}_{nm}\mathbf{U}_{nm}=0,$$

where the prime denotes the derivative with respect to z and the (12×12) matrices are defined by

$$\mathbf{M}_{nm}=\begin{bmatrix}\mathbf{M}^{(1)}_{nm}&0&0\\0&\mathbf{M}^{(1)}_{nm}&0\\0&0&\mathbf{M}^{(2)}_{nm}\end{bmatrix},\qquad \mathbf{N}_{nm}=\begin{bmatrix}0&0&\mathbf{N}^{(1)}_{nm}\\0&0&\mathbf{N}^{(2)}_{nm}\\\mathbf{N}^{(1)}_{nm}&\mathbf{N}^{(2)}_{nm}&0\end{bmatrix},$$

$$\mathbf{P}_{nm}=\begin{bmatrix}\mathbf{P}^{(1)}_{nm}&\mathbf{P}^{(4)}_{nm}&0\\\mathbf{P}^{(4)}_{nm}&\mathbf{P}^{(2)}_{nm}&0\\0&0&\mathbf{P}^{(3)}_{nm}\end{bmatrix},$$

with 4×4 blocks entries given by

$$\mathbf{M}^{(1)}_{nm}=\mu\mathbf{I},\qquad \mathbf{M}^{(2)}_{nm}=(\lambda+2\mu+\eta)\mathbf{I},$$

$$\mathbf{N}^{(1)}_{nm}=(\lambda+\mu)nD^x,\qquad \mathbf{N}^{(2)}_{nm}=(\lambda+\mu)mD^y,$$

$$\mathbf{P}^{(1)}_{nm}=-((\lambda+2\mu+\eta)n^2+\mu m^2)\mathbf{I},$$

$$\mathbf{P}^{(2)}_{nm}=-((\lambda+2\mu+\eta)m^2+\mu n^2)\mathbf{I},$$

$$\mathbf{P}^{(3)}_{nm}=-\mu(n^2+m^2)\mathbf{I},\qquad \mathbf{P}^{(4)}_{nm}=(\lambda+\mu)nmD^xD^y.$$

Computation of the (n,m)-components of the stress tensor gives

$$\sigma_{xx}=\left((\lambda+2\mu+\eta)nD^xU^x_{nm}+\lambda mD^yU^y_{nm}+\lambda(U^z_{nm})'\right)\cdot T_{nm},$$

$$\sigma_{yy}=\left((\lambda+2\mu+\eta)mD^yU^y_{nm}+\lambda nD^xU^x_{nm}+\lambda(U^z_{nm})'\right)\cdot T_{nm},$$

$$\sigma_{zz}=\left((\lambda+2\mu+\eta)(U^z_{nm})'+\lambda(nD^xU^x_{nm}+mD^yU^y_{nm})\right)\cdot T_{nm},$$

$$\sigma_{xy} = \mu\left(nD^x U^y_{nm} + mD^y U^x_{nm}\right) \cdot T_{nm},$$

$$\sigma_{xz} = \mu\left(nD^x U^z_{nm} + (U^x_{nm})'\right) \cdot T_{nm},$$

$$\sigma_{yz} = \mu\left(mD^y U^z_{nm} + (U^y_{nm})'\right) \cdot T_{nm},$$

so that both boundary conditions on the free-surface and interface conditions on the stress, which both involve $\overline{\boldsymbol{\sigma}}(z)\mathbf{e}_z$, can be expressed as linear combinations of $\mathbf{U}_{nm}(z)$ and $\mathbf{U}'_{nm}(z)$, in the form

$$\mathbf{S}_{nm}\mathbf{U}_{nm}(z) + \mathbf{Q}_{nm}\mathbf{U}'_{nm}(z),$$

where

$$\mathbf{S}_{nm} = \begin{bmatrix} 0 & 0 & \mu n D^x \\ 0 & 0 & \mu m D^y \\ \lambda n D^x & \lambda m D^y & 0 \end{bmatrix}, \qquad \mathbf{Q}_{nm} = \begin{bmatrix} \mathbf{M}^{(1)}_{nm} & 0 & 0 \\ 0 & \mathbf{M}^{(1)}_{nm} & 0 \\ 0 & 0 & \mathbf{M}^{(2)}_{nm} \end{bmatrix}.$$

3.5. Boundary conditions and energy estimate

The field equations (6)–(8) thus given have piecewise exponential solutions with respect to z, and integration constants have to be obtained via interface and boundary conditions. The solution for the (n,m)-component in the α-layer will be denoted $\mathscr{U}^{(\alpha)}_{nm}(z) = (\mathbf{U}^{(\alpha)}_{nm}(z), (\mathbf{U}^{(\alpha)}_{nm}(z))')$ so that

$$\mathscr{U}^{(\alpha)}_{nm}(z) = \mathscr{E}^{(\alpha)}_{nm}(z)\mathscr{U}^{(\alpha)}_{nm}(h_{\alpha-1}),$$

where $\mathscr{E}^{(\alpha)}_{nm}(z) = \exp((z - h_{\alpha-1})\mathbf{E}^{(\alpha)}_{nm})$ and

$$\mathbf{E}^{(\alpha)}_{nm} = \begin{bmatrix} 0 & 1 \\ -(\mathbf{M}^{(\alpha)}_{nm})^{-1}\mathbf{P}^{(\alpha)}_{nm} & -(\mathbf{M}^{(\alpha)}_{nm})^{-1}\mathbf{N}^{(\alpha)}_{nm} \end{bmatrix}_{\alpha}.$$

This introduces 24 integration constants $\mathscr{U}^{(\alpha)}_{nm}(h_{\alpha-1})$ for each α. In the following it will be convenient to denote the 12×12 blocks in the expression of $\mathscr{U}^{(\alpha)}_{nm}(z)$ as

$$\mathscr{E}^{(\alpha)}_{nm}(z) = \begin{bmatrix} \mathbf{F}^{(\alpha)}_{nm}(z) & \mathbf{G}^{(\alpha)}_{nm}(z) \\ \mathbf{H}^{(\alpha)}_{nm}(z) & \mathbf{J}^{(\alpha)}_{nm}(z) \end{bmatrix}. \tag{9}$$

At $z = 0$ condition $\overline{\mathscr{P}}_2(b)$ gives

$$\mathbf{U}^{(1)}_{nm}(0) = 0$$

and the continuity of the displacement at $z = h_1$ and formula (9) give

$$\mathbf{G}^{(1)}_{nm}(h_1)(\mathbf{U}^{(1)}_{nm}(0))' = \mathbf{U}^{(2)}_{nm}(h_1).$$

The free-traction condition at $z = h_2$ is

$$\mathbf{S}^{(2)}[\mathbf{F}^{(2)}_{nm}(h_2)\mathbf{U}^{(2)}_{nm}(h_1) + \mathbf{G}^{(2)}_{nm}(h_2)(\mathbf{U}^{(2)}_{nm}(h_1))'] + \mathbf{Q}^{(2)}[\mathbf{H}^{(2)}_{nm}(h_2)\mathbf{U}^{(2)}_{nm}(h_1) + \mathbf{J}^{(2)}_{nm}(h_2)(\mathbf{U}^{(2)}_{nm}(h_1))'] = 0$$

and the continuity of the traction at $z = h_1$ is expressed as

$$\begin{aligned}&[\mathbf{S}^{(1)}\mathbf{G}^{(1)}_{nm}(h_1) + \mathbf{Q}^{(1)}\mathbf{J}^{(1)}_{nm}(h_1)](\mathbf{U}^{(1)}_{nm}(0))' - \mathbf{S}^{(2)}\mathbf{U}^{(2)}_{nm}(h_1) - \mathbf{Q}^{(2)}\mathbf{U}^{(2)}_{nm}(h_1)' \\ &\quad = \sigma^0(-nD_x\Phi^{(1)}_{nm}, -mD_y\Phi^{(1)}_{nm}, 0).\end{aligned} \tag{10}$$

To summarize, the boundary conditions can be expressed for a fixed couple (n,m) as

$$\begin{bmatrix} \mathbf{I} & 0 & 0 & 0 \\ 0 & \mathbf{G}^{(1)} & -\mathbf{I} & 0 \\ 0 & \mathbf{S}^{(1)}\mathbf{G}^{(1)}+\mathbf{Q}^{(1)}\mathbf{J}^{(1)} & -\mathbf{S}^{(2)} & -\mathbf{Q}^{(2)} \\ 0 & 0 & \mathbf{S}^{(2)}\mathbf{F}^{(2)}+\mathbf{Q}^{(2)}\mathbf{H}^{(2)} & \mathbf{S}^{(2)}\mathbf{G}^{(2)}+\mathbf{Q}^{(2)}\mathbf{J}^{(2)} \end{bmatrix} \cdot \begin{bmatrix} \mathbf{U}^{(1)}(0) \\ (\mathbf{U}^{(1)}(0))' \\ \mathbf{U}^{(2)}(h_1) \\ (\mathbf{U}^{(2)}(h_1))' \end{bmatrix} = \begin{bmatrix} 0 \\ 0 \\ \mathbf{K}^{(1)} \\ 0 \end{bmatrix},$$

where $\mathbf{K}^{(1)}$ denotes, for each fixed couple (n,m), the right-hand side of (10), viz.,

$$\mathbf{K}^{(1)} = \sigma^0(-nD_x\Phi^{(1)}_{nm}, -mD_y\Phi^{(1)}_{nm}, 0),$$

while $\mathbf{G}^{(1)}$, $\mathbf{J}^{(1)}$, $\mathbf{F}^{(2)}$, $\mathbf{G}^{(2)}$, $\mathbf{H}^{(2)}$, $\mathbf{J}^{(2)}$ are here, in short, $\mathbf{G}^{(1)}(h_1)$, $\mathbf{J}^{(1)}(h_1)$, $\mathbf{F}^{(2)}(h_2)$, $\mathbf{G}^{(2)}(h_2)$, $\mathbf{H}^{(2)}(h_2)$, $\mathbf{J}^{(2)}(h_2)$ respectively. Turning back to formula (5) we obtain for the elastic energy the estimate

$$\overline{W}_2 = W_0 + \varepsilon^2\frac{\sigma^0}{2}\sum_{n,m=0}^{\infty}\int_{[0,2\pi]^2}\left[n(U^x_{nm}\cdot T_{nm})(D^x\Phi_{nm}\cdot T_{nm}) + m(U^y_{nm}\cdot T_{nm})(D^y\Phi_{nm}\cdot T_{nm})\right]\mathrm{d}x\,\mathrm{d}y$$

and taking into account the orthogonality of the components of T_{nm}, a straightforward computation shows that

$$\overline{W}_2 = W_0 + \varepsilon^2\frac{\sigma^0}{2}\sum_{n,m=0}^{\infty}\left[nD^xU^x_{nm}(h_1) + mD^yU^y_{nm}(h_1)\right]\cdot\overline{\Phi}_{nm}, \tag{11}$$

where $\overline{\Phi}_{nm}$ are obtained by dropping the λ_{nm} in the expression of Φ_{nm}.

4. Applications in semiconductor crystal growth field

Throughout this part, numerical calculations will be performed for three typical couples of semiconductors, viz., Ge/Si, InAs/InP and InAs/GaAs, but this choice does not affect the validity of the above developed method for other types of materials. Therefore, we have collected in Table 1 all the physical data needed for the numerical applications, i.e., the lattice parameters (in nm) and the elastic constants in 10^2 GPa (see Landolt-Bornstein, 1982).

It is straightforward to check that a Ge film is −4.57% compressively strained on a Si substrate, an InAs film −3.2% compressively strained on an InP substrate and an InAs film −7.17% compressively strained on a GaAs substrate. The correspondence between the elastic parameters in Table 1 and those used in the first part of this paper is the following:

$$\lambda = C_{12}, \quad \mu = C_{44} \quad \text{and} \quad \eta = C_{11} - C_{12} - 2C_{44}.$$

Table 1
Numerical values for lattice parameters, elastic constants and anisotropy coefficients for materials considered in the present numerical simulations

	Lattice parameter	C_{11}	C_{12}	C_{44}	α
Si	0.541	1.657	0.639	0.796	0.46
Ge	0.565	1.240	0.413	0.683	0.49
InAs	0.605	0.832	0.452	0.395	0.70
InP	0.586	1.011	0.561	0.456	0.68
GaAs	0.565	1.190	0.538	0.595	0.59

The lattice parameters (in nm), the elastic constants in 10^2 GPa. The anisotropy parameter α is defined in (12) and vanishes for an isotropic material.

Furthermore, for cubic materials an anisotropy coefficient α can be defined using either the formula

$$\alpha = \frac{(2C_{44} + C_{12} - C_{11})(C_{11} + 2C_{12})}{2C_{44}(C_{11} + C_{12})} \tag{12}$$

or using classical linear elasticity notations,

$$\alpha = \frac{1}{E}\left[\frac{1+v}{E} - \frac{1}{2G}\right],$$

where E is the Young's modulus, v is the Poisson ratio and G is the torsion module, so that, for an isotropic material $\alpha = 0$.

Because in a semiconductor crystal, atoms belonging to inner atomic layers far enough from the surface are almost completely unable to reorganize themselves on the crystal sites (because of the activation energy required to break the strong diamond or zinc-blende chemical bonding), buried interface morphology is always considered to be frozen in the following.

4.1. Application (I): growth of a cap-layer

As mentioned in Section 1, when a B layer is coherently grown on an A substrate for example by MBE, the B layer first grows layer-by-layer (2D-growth mode) with an almost *flat surface morphology up to a critical thickness* above which the growth mode changes from this 2D-growth mode to a 3D-growth mode characterized by the formation of coherent islands. These islands are regularly distributed either directly on the A-substrate surface or on a flat B layer (in fact, part of the 2D-grown B layer). This fraction of the B layer which remains flat is called the *wetting-layer*. This growth mode transition is quite well understood *via* the classical explanation given by Grinfeld's method (Grinfeld, 1991; Danescu, 2001).

The next step in the experimental process is generally to grow an A cap-layer on top of this B/$A_{substrate}$ heterostructure to achieve an electron quantum confinement in the B layer (which in that case becomes a *quantum well* in optoelectronic terminology). This A cap-layer is usually lattice-matched with the substrate and therefore mismatched with the buried B layer. There is a lot of experimental evidence showing that during its growth the A cap-layer gradually smoothes out and finally recovers a flat 2D-growth mode even if it had an initially undulated surface (because of the underlying B layer). We shall show in this subsection that according to the above developed formalism, this 2D-growth mode recovery for the A cap-layer can be seen as a straightforward consequence of elastic relaxation in a multi-layered heterostructure.

Let us recall that we have already demonstrated in formula (1) that in a two-layer heterostructure A/B/$A_{substrate}$, the elastic energy difference $W_2 - W_0$ depends only on the displacement on the buried A/B interface (previously denoted $\hat{\Sigma}_1$). However, the surface energy must be taken into account. Considering that the surface energy is almost proportional to the developed area of the upper free-surface (denoted $\hat{\Sigma}_2$), we conclude that the minimum total energy of the system, i.e., surface energy plus elastic energy, is fully determined by the surface energy minimum, that is to say, is obtained for the flat-free surface morphology. In other words, the *cap-layer surface smoothes down as the cap-layer grows*, a qualitative result in agreement with experimental results.

To go further, we have implemented the method developed in Section 3, solved the linearized elastic problem ($\overline{\mathscr{P}}_2$), and finally computed the energy release using formula (11) for the three above mentioned systems: Si/Ge/Si(1 0 0), InP/InAs/InP(1 0 0) and GaAs/InAs/GaAs(1 0 0). Note that in this part, we actually compute $\Delta W = \overline{W}_2 - W_0$ (instead of $\Delta W = \overline{W}_0 - W_2$) so that an energy release is achieved when ΔW is negative in agreement with the convention commonly used by physicists.

In the present case, the system $\overline{W}_2$ under consideration is a reference domain Σ of a stress-free A crystal with spatial dimensions 200 Å × 200 Å. The geometry of the interface $\hat{\Sigma}_1$ between the first B layer and the A cap-layer involves only one Fourier component

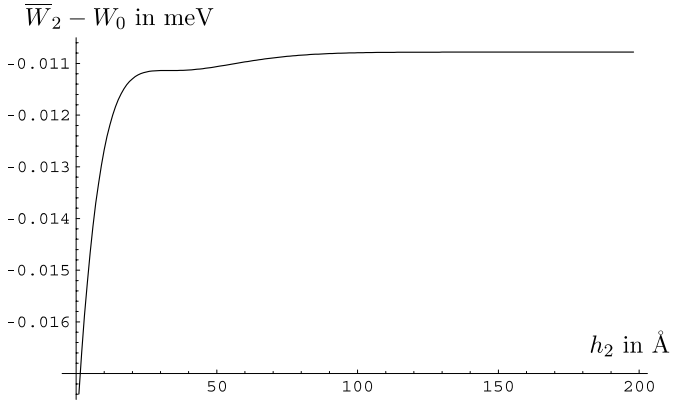

Fig. 2. Elastic energy release as a function of the spacer thickness in a Si/Ge/$Si_{substrate}$ structure; the spacer thickness $h_2 \in (12, 200)$ Å and the thickness of the first B layer, denoted h_1, is 12 Å. A scaling factor ε^2 should be considered for comparison with the experiment, related to the amplitude of the perturbation; here $\varepsilon = 10^{-1}$.

$$\Phi_1(x, y) = \sin\left(\frac{x}{100}\pi\right) \cdot \sin\left(\frac{y}{100}\pi\right)$$

for computational simplicity (but note that this does not mean any loss of generality as may be seen from Section 3). The geometry between the thin film B and the $A_{substrate}$, previously denoted Σ_0, is assumed to be flat. The reference system W_0 is a system with the same amount of material but with all interfaces flat.

First we chose a typical thickness maximum $h_1 = 12$ Å for the B layer and we varied the thickness h_2 of the A cap-layer in the range (12, 200) Å, in order to analyze the effect on the elastic energy release. The normalized energy differences ΔW (negative, as expected) versus the cap-layer thickness h_2 are plotted in Fig. 2 for Si/Ge/$Si_{substrate}$. The results obtained for InP/InAs/$InP_{substrate}$ and GaAs/InAs/$GaAs_{substrate}$ respectively, have the same qualitative features.

At the beginning of the A cap-layer growth, ΔW strongly increases, indicating that part of the energy release obtained by undulating the B layer is now partially wiped away for the system because of the mismatched interface between the A cap-layer and the B layer. The B layer no longer has a free surface able to relax elastic energy. However, ΔW tends to an asymptotic negative value indicative of an energy release. This upper bound for the energy release clearly depends on the geometry of the buried B layer.

4.2. Applications (II): optimal vertical self-organization

Today, stacking processes are widely-used approaches to improve strain-induced quantum island self-organization. They consist in the over-growth of a new B layer on the A/B/$A_{substrate}$ heterostructure discussed above, yielding to a new B/A/B/$A_{substrate}$ heterostructure. Consequently, the previous cap-layer is renamed and becomes *a spacer-layer* since it is now in between two B layers. On the one hand, such a stacking process strongly enhances the lateral self-organization, a fact that can be perceived here as an improvement of the modulation periodicity. On the other hand, the strain distribution due to the islands of the buried B-layer induces a vertical alignment of the latter with those of the above grown B-layers (Xie et al., 1995; Tersoff et al., 1996; Zhang et al., 1999; Priester, 2001). This top-on-top situation will be called in the present formalism *in-phase* or *correlated*. As an illustration, Fig. 3 represents three successive vertically *correlated* layers (left picture) and three successive vertically *anti-correlated* layers (right picture) respectively. If the stacking process is repeated to make superlattices from the elementary motif, it usually results in vertical heaps of well-organized islands.

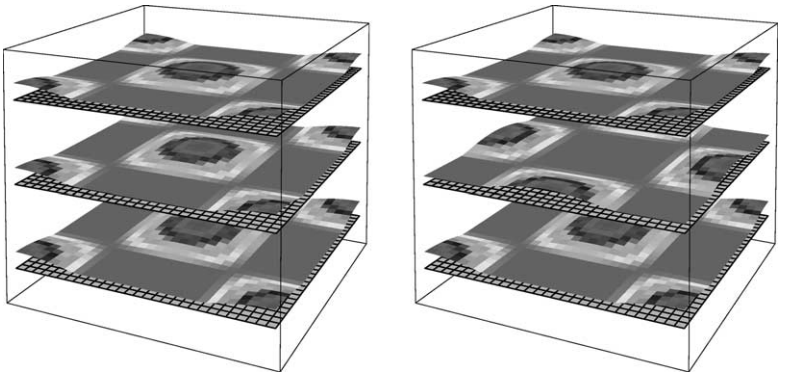

Fig. 3. A generic example of three vertical correlated layers (left picture) and three vertical anti-correlated layers (right picture).

For convenience, Fig. 3 captures only the shape of the undulated A/B interfaces, all B/A interfaces being flat. For systems grown along (1 0 0) substrates, experiments Solomon et al. (1996), Teichert et al. (1996), Legrand et al. (1999), Lita et al. (1999), Wu et al. (1997) have clearly shown that this kind of *vertical dot alignment prevails* for systems like Ge/Si, InAs/InP or InAs/GaAs. However, in a recent letter (Holý et al., 1999), it has been claimed that this usual vertical correlation can be affected by a strong elastic anisotropy leading to a non-top-on-top dot stacking, called here *anti-correlation*. Our concern in this subsection is thus to obtain, using the previous method, some insight concerning the following questions:

(Q1) Is the current formalism able to capture the main features of the rather complex elastic interaction between two strained B-layers separated by an A-spacer?
(Q2) Is the top-on-top vertical correlation more favourable than non-top-on-top vertical correlation even for structures involving strong anisotropic materials?
(Q3) Is there a critical spacer thickness for which the elastic energy release is optimum?

4.2.1. Vertical correlation versus anti-correlation

In this subsection we shall answer the first two questions, by considering in the following a superlattice B/A/B/$A_{substrate}$. We have implemented the semi-analytical method exposed in Section 3 and studied the role of the vertical arrangement of islands between two neighboring B layers separated by an A material spacer. For fixed $(x_0, y_0) \in [0, \pi]^2$ we compute the elastic energy release $\Delta W = \overline{W}_3 - W_0$ for Ge/Si/Ge/$Si_{substrate}$ in a situation where the geometry of the upper surfaces of B layers, namely $\hat{\Sigma}_1$ and $\hat{\Sigma}_3$ are defined by

$$\Phi_1(x, y) = \sin\left(\frac{x}{100}\pi\right)\sin\left(\frac{y}{100}\pi\right)$$

and

$$\Phi_3(x, y) = \sin\left(\frac{x + x_0}{100}\pi\right)\sin\left(\frac{y + y_0}{100}\pi\right),$$

respectively, while the upper surfaces of the A layers are considered flat. This is consistent with an initial deposition on a flat substrate and with our previous results concerning the 2D growth recovery of the cap-layer.

The symmetry properties of Φ_1 and Φ_3 allow us to compute values ΔW only on $(0, \pi) \times (0, \pi)$. The first computation was performed on a grid containing 2500 points (50×50) for Ge/Si/Ge/$Si_{substrate}$ with Ge dot-layers and a Si spacer-layer thickness of 15 and 48 Å respectively. The results $\Delta W(x_0, y_0)$, which is a scalar function of two variables (x_0, y_0), are plotted in Fig. 4 using a plane map with gray-level scaling proportional to the difference $\overline{W}_3 - W_0$ such that the favourable situation, i.e. small ΔW, is dark. Fig. 4 clearly

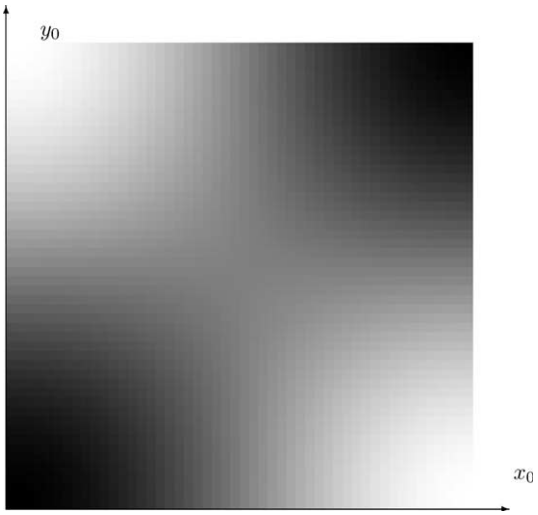

Fig. 4. The normalized elastic energy release $\Delta W(x_0, y_0)$ for a three-layered material Ge/Si/Ge/$Si_{substrate}$; the thickness of successive Ge/Si/Ge layers is (15, 48, 15) Å respectively. The dark-level indicates a favourable site (small ΔW) so that this computation shows that vertical *correlation* is energetically more favourable than vertical *anti-correlation*. The symmetry of the gray-level reflects the symmetry of the elastic problem.

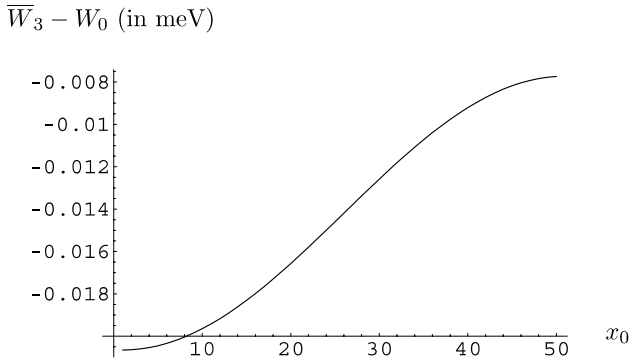

Fig. 5. Profile curve obtained as a section in Fig. 4 for $y_0 = 0$; once again a scale factor $\varepsilon = 10^{-1}$ in formula (11) was considered.

shows that the vertical alignment is the most favourable situation. To have a quantitative picture Fig. 5 displays the corresponding profile curve obtained at $y_0 = 0$.

Similar results have been obtained for InAs/InP/InAs/$InP_{substrate}$ and InAs/GaAs/InAs/$GaAs_{substrate}$. Once again the only observed difference concerns a scale effect, as expected for systems having neither the same lattice mismatch nor the same elastic constants. We conclude that *under our current hypothesis vertical correlation is more favourable than vertical anti-correlation, in agreement with most actual experiments.*

4.2.2. Optimum spacer thickness

In this subsection we focus on the effect of the A spacer thickness on the elastic energy release of the energetically most favourable situation determined above, i.e., the vertical island correlation for which both upper surface and the first A/B interface are given by

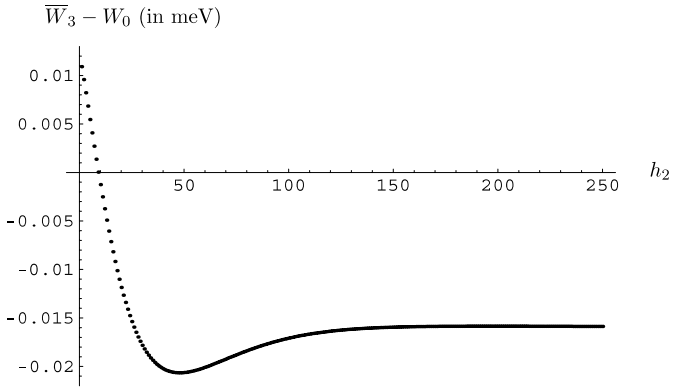

Fig. 6. Normalized energy release as a function of the spacer thickness h_2 for $h_2 \in (12, 250)$ Å, for $h_1 = h_3 = 12$ Å.

$$\Phi_1(x,y) = \Phi_3(x,y) = \sin\left(\frac{x}{100}\pi\right)\sin\left(\frac{y}{100}\pi\right).$$

As a result the elastic energy difference $\Delta W = \overline{W}_3 - W_0$ as a function of the A-spacer thickness for the Ge/Si case is shown in Fig. 6.

For a three-layer material of type B/A/B/$A_{substrate}$ the elastic energy release due to the corrugation of both interface A/B and free-surface can be seen as the sum of three terms: the first one corresponds to the stress relaxation of the lower B-layer; the second one is the same but for the upper B-layer and the third one is an interaction term. The main qualitative features in Fig. 6 can be explained as follows. When the A-spacer is thin, the interaction between the two close neighboring B-layers yields to a large elastic energy in the system because of a high shear contribution in the A-spacer. When the spacer is thicker, the elastic energy release gained by the stress relaxation of the B-layers dominates this interaction term, and the total elastic energy of the corrugated structure becomes less than that of the structure with flat interfaces. The balance is reached when the energy of the corrugated structure equals that of the structure with flat interfaces, that is to say, when $h_2 \sim 10$ Å for perturbation amplitudes of 1 Å. An optimum for the energy release is attained at $h_2 \sim 50$ Å. After this point the curve slightly increases up to an asymptotic value corresponding to no interaction at all between the two B-layers. We conclude that there is an optimum spacer thickness for which the interaction of the B-layers allows the maximum elastic energy to be relaxed.

As already noted in experiments, this elastic energy minimum is clearly related to the geometrical characteristics of the undulated B-layer, and especially to its period. In brief, these numerical results indicate that the layer interaction energy is of the same magnitude as the elastic energy release for a single layer. Actually, this implies that there is an optimum compromise between spacer thickness and strained-layer relative undulations to relax maximum elastic energy.

5. Concluding remarks

A continuum mechanics approach based on a generalization of Grinfeld's method has been developed to calculate the elastic energy for multi-layer heterostructures like those actually grown by MBE for opto-electronic device engineering. A semi-analytical solution using a small-amplitude perturbation approximation and Fourier analysis has been proposed.

In the second part special emphasis has been put on the study of superlattices alternating layers of coherently strained dots with spacer layers which are lattice-matched with a semi-infinite substrate. We have shown that an energy release can be obtained by undulating the strained layer even if buried under a cap-layer. By contrast, there is no energy requirement for the cap-layer free surface to undulate owing to

the increase of the subsequent surface energy. In other words, the total energy minimum for a system involving a strained layer buried under a cap-layer is an undulation for the strained buried layer but a flat surface for the cap-layer. The mechanism of interaction between two undulated strained layers separated by a spacer layer has also been investigated.

The main result concerns the staking mode (either in-phase or out-of-phase) of the undulations. We found that the in-phase one is the most energetically favourable mode even for strongly anisotropic material. More to the point, a study of the energy release process versus spacer-layer thickness clearly demonstrates the way the strained layers interact and relax. To be more precise, if the undulated strained layer are close enough to strongly interact, the contribution of the interaction between them to the elastic energy can overwhelm the energy gain due to their own layer undulations. In this case, it is energetically more favourable for the system on the whole to have no undulations at all for the strained layers than to have non-propitious shear stresses into the spacer-layer. As the spacer layer thickness increases, the energy balance becomes more and more favourable to undulations for the strained layers up to an optimum thickness. Finally when there is no interaction between the undulated strained layers because they are too far away from each other, the correlated or anti-correlated undulated modes become equally good and both energetically favourable.

References

Danescu, A., 2001. The Asaro–Tiller–Grinfeld instability revisited. Int. J. Solids Struct. 38, 4671–4684.

Grinfeld, M.A., 1986. Sov. Phys. Dokl. 31, 831.

Grinfeld, M.A., 1991. Thermodynamic Methods in the Theory of Heterogenous Substances. Longman, London.

Grinfeld, M.A., 1993. The stress driven instabilities in crystals: mathematical models and physical manifestations. J. Nonlinear Sci. 3, 35–83.

Holý, V., Springholz, G., Pinczolits, M., Bauer, G., 1999. Strain induced vertical and lateral correlations in quantum dot superlattices. Phys. Rev. Lett. 83, 356–359.

Landolt-Bornstein, 1982. In: Madelung, O. (Ed.), Numerical Data and Functional Relationships in Science and Technology. Springer-Verlag, Berlin.

Legrand, B., Nys, J.P., Grandidier, B., Stievenard, D., Lemaitre, A., Gerard, J.M., Thierry-Mieg, V., 1999. Quantum box size effect on vertical self-alignment studied using cross-sectional scanning tunneling microscopy. Appl. Phys. Lett. 74, 2608–2610.

Lita, B., Goldman, R.S., Phillips, J.D., Bhatacharya, P.K., 1999. Nanometer-scale studies of vertical organization and evolution of stacked self-assembled InAs/GaAs quantum dots. Appl. Phys. Lett. 74, 2824–2826.

Priester, C., 2001. Vertical correlations and anticorrelations in multisheet arrays of two-dimensional islands. Phys. Rev. B 63, 153303.

Shchukin, V.A., Bimberg, D., Malyshkin, V.G., Ledentsov, N.N., 1998. Vertical correlations and anticorrelations in multisheet arrays of two-dimensional islands. Phys. Rev. B 57, 12262–12274.

Shilkrot, L.E., Srolovitz, D.J., Tersoff, J., 2000. Dynamically stable growth of strained-layer superlattices. Appl. Phys. Lett. 77, 304–306.

Solomon, G.S., Trezza, J.A., Marshall, A.F., Harris, J.S., 1996. Vertically aligned and electronically coupled growth Induced InAs islands in GaAs. Phys. Rev. Lett. 76, 952–955.

Spencer, B.K., Voorhees, P.W., Tersoff, J., 2001. Phys. Rev. B 64, 235318.

Springholz, G., Holý, V., Pinczolits, M., Bauer, G., 1998. Self-organized growth of three-dimensional quantum-dot crystals with fcc-like stacking and a tunable lattice constant. Science 282, 734–737.

Teichert, C., Lagally, M.G., Peticolas, L.J., Bean, J.C., Tersoff, J., 1996. Stress-induced self-organization of nanoscale structures in SiGe/Si multilayer films. Phys. Rev. B 53, 15334.

Tersoff, J., Teichert, C., Lagally, M.C., 1996. Self-organization in growth of quantum dot superlattices. Phys. Rev. Lett. 76, 1675–1678.

Wu, W., Tucker, J.R., Solomon, G.S., Harris, J.S., 1997. Atom-resolved scanning tunneling microscopy of vertically ordered InAs quantum dots. Appl. Phys. Lett. 71, 1083–1085.

Xie, Q., Madhukar, A., Chen, P., Kobayashi, N.P., 1995. Vertically self-organized InAs quantum box islands on GaAs(1 0 0). Phys. Rev. Lett. 75, 2542–2545.

Zhang, Y.W., Xu, S.J., Chiu, C.H., 1999. Vertical self-alignment of quantum dots in superlattice. Appl. Phys. Lett. 74, 1809–1811.